

Isolation and Structural Characterization of Stable Carbamic-Carbonic Anhydrides: An Experimental and Computational Study

Ivo E. Sampaio-Dias,^{a,} Carlos A. D. Sousa,^b Sara C. Silva-Reis,^a*

Luís Pinto da Silva,^{c,d} Xerardo García-Mera,^e and José E. Rodríguez-Borges^a

^aLAQV/REQUIMTE, Department of Chemistry and Biochemistry, Faculty of Sciences, University of Porto, R. Campo Alegre 697, 4169-007 Porto, Portugal.

^bCIPAN - Companhia Industrial Produtora de Antibióticos, SA; R. da Estação 42, Castanheira do Ribatejo, Portugal.

^cChemistry Research Unit (CIQUP), Faculty of Sciences, University of Porto, R. Campo Alegre 697, 4169-007 Porto, Portugal.

^dLACOMEPhi, GreenUPorto, Department of Geosciences, Environment and Territorial Planning, Faculty of Sciences, University of Porto, R. Campo Alegre 697, 4169-007 Porto, Portugal.

^eDepartment of Organic Chemistry, Faculty of Pharmacy, University of Santiago de Compostela, E-15782 Santiago de Compostela, Spain.

*Corresponding author e-mail: idias@fc.up.pt.

Abstract

Carbamic-carbonic anhydrides are elusive species that have been only indirectly detected under controlled conditions. This functional group is transiently formed during the reaction of secondary amines with anhydrides in the presence of nucleophilic catalysts such as 4-(dimethylamino)pyridine. In this work, the synthesis and isolation of two carbamic-carbonic anhydrides are reported, including the first-ever solid-state structure of this functional group. The remarkable stability of these chiral carbamic-carbonic anhydrides allowed their study by NMR, HRMS, FTIR-ATR, and thermal analysis techniques (DSC and TGA). A thorough analysis of the bonding situation by computational studies hint that the origin of its unusual stability relies on $n \rightarrow \sigma^*$ stabilizing orbital interactions hampering decarboxylation to occur.

Introduction

Carbamic-carbonic anhydrides combine carbamic and carbonic acid moieties into an anhydride-like arrangement (Fig. 1B).¹⁻³ Despite these compounds having been known for several decades as intermediates of the reaction of secondary amines with anhydrides in the presence of nucleophilic catalysts such as 4-(dimethylamino)pyridine (DMAP), the chemistry of carbamic-carbonic anhydrides remains poorly studied. These compounds are generally highly unstable and readily prone to decarboxylation to generate the corresponding carbamates (Fig. 1B), making isolation and characterization of these species a herculean task.² In 1971, Dean and Tarbell have proposed the formation of carbamic-carbonic anhydrides as intermediates from the reaction between tricarbonates with secondary amines.³ Later on, in 1988, Kemp and Curran were the pioneers in the detection of a carbamic-carbonic anhydride as an unstable intermediate during the acylation of the *trans* isomer of 2,5-dicarbethoxypyrrolidine with di-*tert*-butyl dicarbonate (Boc₂O) in the presence of DMAP.¹

In a landmark study,² Basel and Hassner have investigated in detail the protection of different primary and secondary alkylamines (Figs. 1A and 1B, respectively) as well as anilines with Boc₂O in the presence and absence of DMAP,² and established the major products associated with these reactions. By employing catalytic amounts of DMAP, primary amines are known to afford the expected *N-tert*-butyloxycarbonyl (*N*-Boc) carbamates along with urea and isocyanate as side products (Fig. 1A).² The distribution of the products depends on the temperature, with the isocyanate being the major product at lower temperatures (Fig. 1A).²

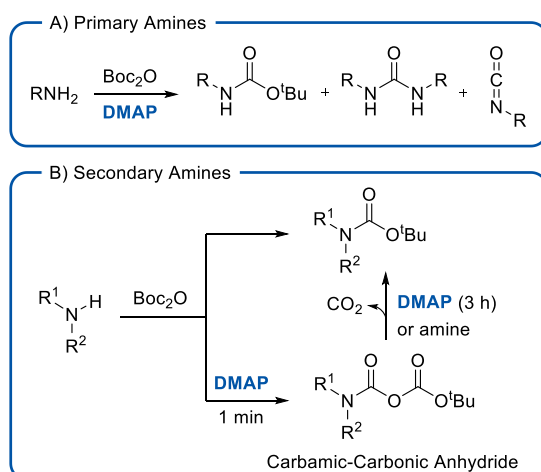


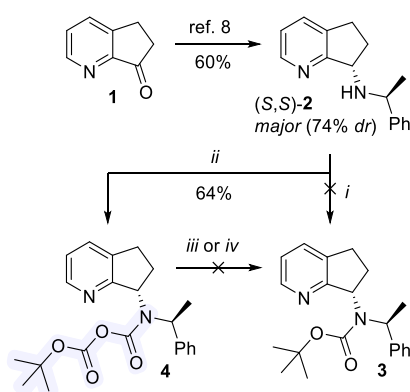
Fig. 1. Reaction of primary and secondary alkylamines with Boc₂O-DMAP.²

In contrast, secondary amines react with Boc₂O and DMAP to afford exclusively the corresponding carbamates (Fig. 1B). By quenching the reactions after 1-5 min using 1% HCl, Basel and Hassner were able to successfully detect these underexplored anhydrides by NMR analyses directly from the reactional crude (without purification by column chromatography) due to their intrinsic lability.² These findings were further supported by reacting the carbamic-carbonic anhydrides with DMAP (3 h) or after the addition of the starting amine, forming the desired carbamates upon decarboxylation (Fig. 1B).²

A survey at Cambridge Structural Database using the ConQuest software reveals that solid-state structures of carbamic-carbonic anhydrides are unknown.⁴ Here we fill this gap and gain more insights on this underexplored functional group by reporting the synthesis of a chiral carbamic-carbonic anhydride with remarkable stability, its characterization in the solid state, and a thorough analysis of the bonding situation.

Results and Discussion

Recently, our research group has been exploring the use of chiral bicyclic amines type **2** (Scheme 1) and its derivatives for the synthesis of Rasagiline analogues⁵⁻⁷ and the development of chiral ligands for asymmetric catalysis.⁸



Scheme 1. Synthesis of chiral carbamic-carbonic anhydride **4**. *Reagents and conditions:* i) Boc₂O, Et₃N, CH₂Cl₂; ii) Boc₂O, DMAP (cat.), CH₂Cl₂; iii) DMAP; iv) heating (up to 140 °C).

Following a regioselective protocol developed by us,⁵⁻⁸ ketone **1** is readily prepared with a 45% global yield (over 4 steps) from 6,7-dihydro-5*H*-cyclopenta[*b*]pyridine. Reductive amination of ketone **1** with (*S*)-1-phenylethan-1-amine in the presence of NaBH(OAc)₃ as the hydride reducing agent afforded amine (*S,S*)-**2** as the major diastereoisomer after column chromatography (60% yield, 74% of diastereoisomeric excess, determined by ¹H-NMR of the crude reaction mixture).⁸ With this chiral amine in hand, we explored the *N*-protection of (*S,S*)-**2** into the *N*-Boc derivative **3** using Boc₂O in the presence of triethylamine (Et₃N). However, contrary to our expectations, all attempts to synthesize carbamate **3** (equimolar and excess amounts of Boc₂O and Et₃N), did not produce any products, with full recovery of the starting amine. Despite *N*-Boc derivatives can be obtained directly from the reaction between aliphatic primary and secondary amines with Boc₂O,⁹ the use of catalysts such as DMAP is widely employed as a standard protocol.^{2, 10-21} In this sense, catalytic amounts of DMAP were used as an Et₃N substitute. After reacting for 5 min a new spot on TLC was found, with no changes in the TLC elution profile when the reaction time was extended up to 4 h.

After the workup (liquid-liquid extraction with an aqueous saturated solution of NaHCO₃) and purification (column chromatography) the solid obtained was analyzed by FTIR-ATR (Fig. 2A).

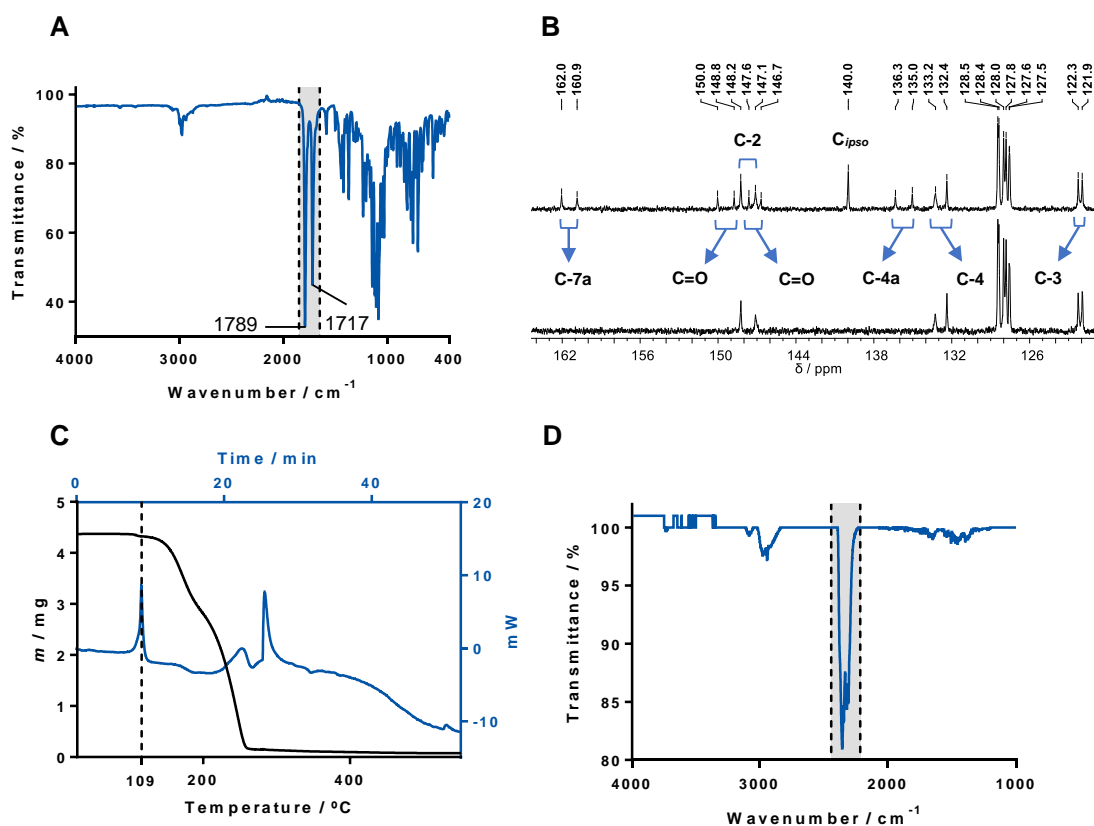


Fig. 2. (A) FTIR-ATR spectrum of **4**; (B) Truncated ¹³C{¹H} NMR (above) and DEPT-135 (under) spectra (100 MHz, CDCl₃) of **4**; (C) TGA/DSC of **4** with detection of CO₂ by FTIR (D) at 15 min.

Surprisingly, the FTIR-ATR spectrum shows two bands of C=O stretch at 1789 and 1717 cm^{-1} (Fig. 2A). This led us to suspect the isolation of a carbamic-carbonic anhydride intermediate **4** instead of the expected carbamate **3**. The ^1H NMR (Fig. S3) and $^{13}\text{C}\{^1\text{H}\}$ NMR (Figs. 2B and S4) data show the presence of two different species in solution (CDCl_3) in a 50:50 ratio (Fig. S3). Regarding that the starting amine (*S,S*)-**2** is diastereoisomerically pure, the origin in the splitting pattern found in the NMR data of **4** is attributed to *cis-trans* conformers in the solution-phase.

A close inspection of the $^{13}\text{C}\{^1\text{H}\}$ and DEPT-135 NMR spectral data indicate the successful isolation of carbamic-carbonic anhydride as a mixture of two conformers (Fig 2B and S4). Note that each conformer displays two quaternary carbons (C=O) in $^{13}\text{C}\{^1\text{H}\}$ NMR (Figs. 2 and S4), which are attributed to the carbonyl carbons of the carbamic-carbonic anhydride motif.² Basel and Hassner have previously documented the presence of conformers in *N*-(*tert*-butyloxycarbonyloxy)carbonyl-*N*-benzylethanamine, showing two sets of quaternary carbons (150.4/149.5 and 147.7/147.6 ppm) in $^{13}\text{C}\{^1\text{H}\}$ NMR,² which agrees with the spectroscopic data found for anhydride **4** (150.0/148.8 and 147.6/146.7 ppm), as depicted in Figs. 2B and S4.

The remarkable isolation of carbamic-carbonic anhydride **4** by chromatography suggests unusual stability for this compound. In fact, anhydride **4** is unaffected by atmospheric moisture and oxygen, with no noticeable conversion to the corresponding carbamate after storage for several months. To best characterize anhydride **4**, thermal analysis techniques such as TGA and DSC coupled to FTIR were performed to identify the thermal decomposition pattern (Figs. 2C and 2D). The DSC shows an endothermic signal at 109.16 $^\circ\text{C}$, which corresponds to the melting point of **4** as confirmed by TGA analysis (Fig. 2C). At higher temperatures (140 $^\circ\text{C}$) in TGA, a noticeable mass loss is detected (33.7%) which is compatible with the complete removal of the anhydride moiety with the subsequent formation of amine **2**. This was further supported by FTIR analysis which unequivocally shows the detection of CO_2 during 11-18 min (Fig. 2D) with a maximum at 15 min, which perfectly matches with the loss of the mass detected by TGA analysis. Both melting and decomposition were confirmed experimentally by warming **4** at 109 and 140 $^\circ\text{C}$ for 1 min, respectively, followed by NMR analysis (Figs. S5 and S6). The ^1H NMR data unequivocally shows no differences between the spectra before and after warming **4** at 109 $^\circ\text{C}$ (Fig. S5). In contrast, the ^1H NMR spectrum obtained after heating **4** at 140 $^\circ\text{C}$ shows appreciable decomposition with

the detection of a mixture of **2** and **4** (Fig. S6) in a ratio of 67:33, respectively, with no noticeable formation of the *N*-Boc counterpart **3** whatsoever.

Attempts to obtain suitable crystals of **4** for X-ray analysis were made to unravel the solid-state structure of this *not-so-labile* derivative. Delightfully, colourless crystals were obtained from slow evaporation of **4** in CH₂Cl₂/CH₃OH 4:1, enabling the study of a carbamic-carbonic anhydride structure for the first time in the solid-state by X-ray crystallography. The ORTEP diagram of the carbamic-carbonic anhydride **4** is shown in Fig. 3.²²

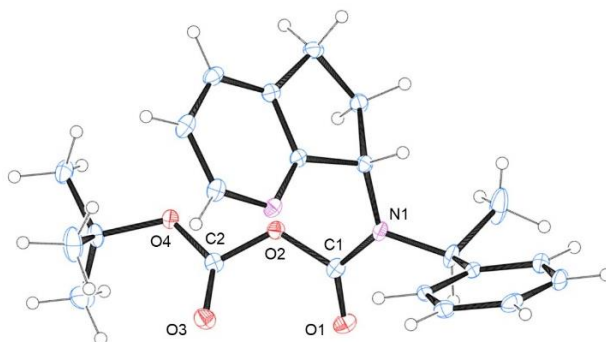
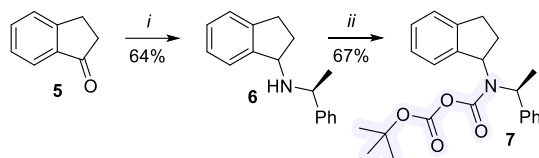


Fig. 3. Single-crystal X-ray diffraction experiment for carbamic-carbonic anhydride **4**. ORTEP diagram for **4** with thermal ellipsoids drawn at 50% probability including an arbitrary numbering system for the carbamic-carbonic anhydride moiety exhibiting a *cis*-conformation. Selected bond distances (Å) for **4**: N1-C1, 1.343; C1-O1, 1.199; C1-O2, 1.402; C2-O2, 1.364; C2-O3, 1.193; C2-O4, 1.309. Color key: blue = C; red = O; pink = N; white = H.

The successful isolation of **4** from **2** as a stable species using standard protocols^{2, 10-21} for *N*-Boc protection of secondary amines with Boc₂O and DMAP as the catalyst raises an important question: may this be an exceptional case or may carbamic-carbonic anhydrides be more common as formal products rather than intermediates? Considering the presence of the basic nitrogen atom in **2** (pyridine moiety), more experiments were conducted to enlighten whether this is (or not) a structural requirement for the formation and stabilization of carbamic-carbonic anhydrides such as **4**. To clarify this point, secondary amine **6** was synthesised from 2,3-dihydro-1*H*-inden-1-one (**5**) and further reacted with Boc₂O in the presence of catalytic amounts of DMAP (Scheme 2).



Scheme 2. Synthesis of carbamic-carbonic anhydride **7**. *Reagents and conditions:* i) (*S*)-1-phenylethan-1-amine, NaBH(OAc)₃, DCM; ii) Boc₂O, DMAP (cat.), CH₂Cl₂.

Using the reductive amination protocol, ketone **5** was converted into secondary amine **6** with 64% yield as a mixture of diastereoisomers in a 93:7 ratio (as determined by NMR, Figs. S7 and S8) after chromatography. Following the procedure employed for the preparation of carbamic-carbonic anhydride **4**, amine **6** was reacted with Boc₂O in the presence of catalytic amounts of DMAP. After 4 h reacting, the TLC showed the formation of a sole product which was isolated by chromatography. Analogously to carbamic-carbonic anhydride **4**, the ¹H NMR spectrum (CDCl₃, Fig. S9) exhibits duplication of the signals in a ratio of 71:29. Furthermore, two sets of quaternary carbons (150.4/150.4 and 148.0/146.9 ppm) were detected in the ¹³C{¹H} NMR (CDCl₃, Fig. S10), which agrees with the spectroscopic data found for anhydride **4**, corroborating the formation of carbamic-carbonic anhydride **7**.²

Variable-temperature NMR experiments (Figs. 4 and S11) in DMSO-*d*₆ unequivocally show the coalescence of signals of **7** from 25 to 80 °C, corroborating the presence of conformers at 25 °C. From 90 to 100 °C it is possible to notice the continuous process of coalescence and the presence of additional signals in the NMR spectra which is associated with the thermal decomposition of carbamic-carbonic anhydride **7** into **6**.

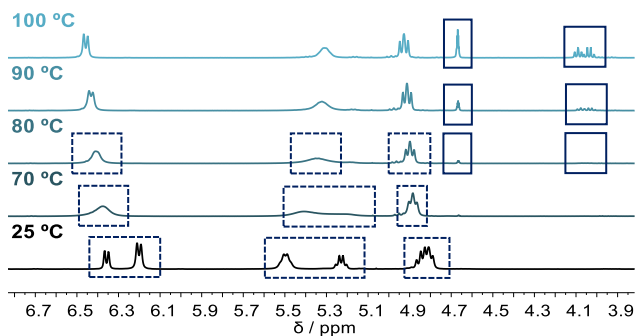
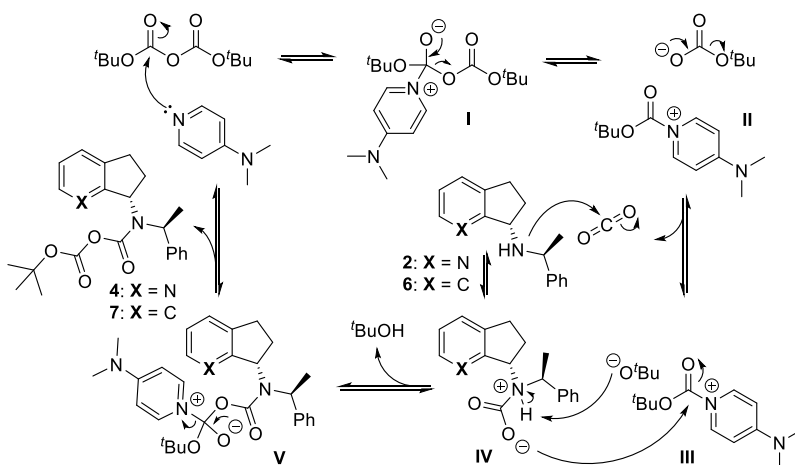


Fig. 4. Truncated ^1H NMR spectra of variable-temperature experiments (400 MHz, $\text{DMSO-}d_6$) for carbamic-carbonic anhydride **7** at 25, 70, 80, 90, and 100 $^\circ\text{C}$. Dashed boxes denote the coalescence of signals with temperature and solid boxes indicate the signals from the decomposition of **7** at higher temperatures.

The successful isolation and characterization of **7** unarguably rule out a potentially critical role of pyridine moiety in (*S,S*)-**2** for the formation and stabilization of **4**. Thus, the formation and isolation of **4** and **7** under this protocol should not be regarded as particular cases, drawing attention to the possibility of the formation of such species as sole formal products.

A plausible mechanism for the formation of carbamic-carbonic anhydrides **4** and **7** is shown in Scheme 3.



Scheme 3. A plausible mechanism for the formation of carbamic-carbonic anhydrides **4** and **7**.

Initially, DMAP reacts with Boc_2O to generate the *N*-Boc-DMAP intermediate **II** and *tert*-butyl carbonate. The isolation of the *N*-Boc-DMAP salts was previously described by Guibé-Jampel and Wakselman,²³ while the spectroscopic identification of the Boc_2O /catalyst complex was performed by Knölker and co-workers.²⁴ Subsequently, *tert*-butyl carbonate undergoes decarboxylation to generate CO_2 *in situ*,²⁵ along with the formation

of intermediate **III**. Despite being a strong electrophile, intermediate **III** seems not to react with amines **2** and **6**, otherwise, the formation of carbamate products would be expected. Since no carbamates were detected in these reactions, it is surmised that CO₂ is trapped by amines **2** or **6** (carbonatation) instead, delivering the corresponding carbamic ions type **IV**. These, in turn, react with *N*-Boc-DMAP intermediate **III** to deliver the carbamic-carbonic anhydrides **4/7**, with the regeneration of the catalyst.

Computational Studies

Regarding the exclusive occurrence of the *cis*-conformer of **4** in the solid-state (Fig. 3), the first aim of the theoretical calculations was to elucidate the presence of two conformers in the solution (CDCl_3) as indicated by NMR data. Two conformers with identical energies (Fig. 5) were identified, which major difference relies on the dihedral ω associated with the *cis*-*trans* isomerization of the carbonyl groups of the carbamic-carbonic anhydride moiety. More specifically, it was found $\omega = 52.3^\circ$ for the *cis* species and $\omega = -102.9^\circ$ for the *trans*-species. Frequency calculations indicated that the *cis* species is more stable than the *trans*-species by just $0.3 \text{ kcal mol}^{-1}$ (Gibbs free energy with thermal corrections), which agrees with the 50:50 ratio of conformers determined experimentally by NMR and the presence of the *cis*-species (more stable) in the solid-state.

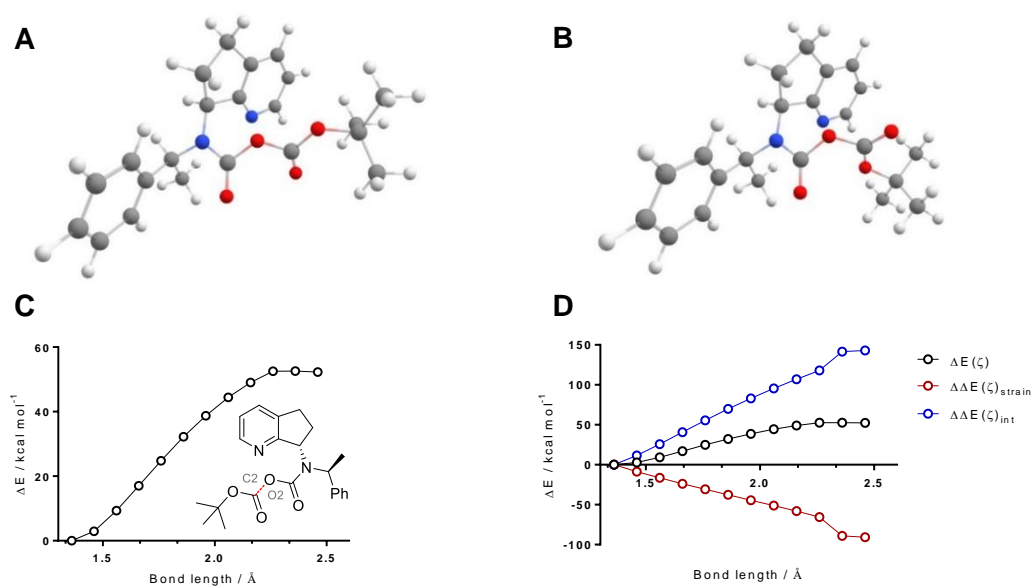


Fig. 5. Optimized geometries, at the $\omega\text{B97XD}/6\text{-}31\text{+G(d,p)}$ level of theory, for the *cis* (**A**) and *trans* (**B**) species of the carbamic-carbonic anhydride **4** (color key: blue = N; red = O; gray = C; white = H). Potential energy curve (**C**) of the C2-O2 bond breaking of the *cis*-species of **4**, as a function of the C2-O2 bond length (steps of 0.1 \AA). Geometry optimized at a fixed bond length of 2.46 \AA , demonstrating the fragmentation into the carbamic ion, CO_2 , and carbocation moieties. (**D**) $\Delta E(\zeta)$, $\Delta\Delta E(\zeta)_{\text{strain}}$ and $\Delta\Delta E(\zeta)_{\text{int}}$ values plotted as a function of the C2-O2 bond length (steps of 0.1 \AA) for the *cis*-species of **4**. All calculations were made at the $\omega\text{B97XD}/6\text{-}31\text{+G(d,p)}$ level of theory in implicit chloroform.

Having identified the origin of the two conformers of carbamic-carbonic anhydride **4**, efforts were made to understand the surprising stability of this compound that, contrary to expectations, does not decompose into the corresponding carbamate and CO₂.²⁶ Thus, firstly, the Gibbs free energy differences (with thermal corrections) between both conformers (*cis* and *trans* species) and their expected decomposition products (carbamate and CO₂) were calculated. Interestingly, and in apparent contrast with experimental data, both decomposition reactions appear to be favorable by 16.6 kcal mol⁻¹ (for the *trans*-species) and by 16.8 kcal mol⁻¹ (for the *cis*-species). This indicates that the reason for the stability of this carbonic anhydride is not related to the exothermicity (or lack thereof), but possibly with high energy barriers present in different reaction steps.

Working on carboxylic-carbonic anhydrides, Tarbell and Leister have suggested an S_N1-type reaction mechanism initiated by C-O bond breaking, leading to the formation of an arylcarboxylic acid moiety, a carbocation, and CO₂.^{26, 27} Upon release of CO₂, recombination of the arylcarboxylate and the carbocation would lead to the formation of the corresponding ester.^{26, 27} Using the same rationale, the potential energy curves of the C2-O2 bond breaking for each conformer were analyzed. This was done by optimizing the geometries of the conformers at several lengths of the relevant C2-O2 bond. The potential energy curves for the *cis* species are present in Fig. 5C, while for the *trans*-species these are present in Fig. S14.

As the C2-O2 bond length increases, the respective energy increases as well for both conformers (Figs. 5C and S14). For the *cis* species, the energy increases continuously up to 52.6 kcal mol⁻¹, with the increase in the C2-O2 from 1.36 to 2.46 Å. At this point, the carbamic-carbonic anhydride is decomposed into the carbamic ion, CO₂, and carbocation species. The results are identical for the *trans*-species, as the energy also increases significantly up to 35.7 kcal mol⁻¹. Given the potential energy curves obtained (Figs. 5C and S14), we propose that the unusual stability of **4** resides on C2-O2 bond-breaking step, which is too energetically demanding. This prevents the CO₂ release and the recombination of the carbamic ion and the *tert*-butyl carbocation to form the corresponding carbamate.

Having provided evidence to support the unexpected stability of carbamic-carbonic anhydride, we proceeded to clarify why the C2-O2 bond breaking is so unfavorable. To this end, we have used the activation strain model,²⁸ also known as the distortion/interaction model.²⁹⁻³¹ This model decomposes the potential energy surface $\Delta E(\zeta)$ into two main contributions along the reaction coordinate ζ : the reaction strain ($\Delta E(\zeta)_{\text{strain}}$), which is determined by structural distortion that the reactants undergo during the reaction; and $\Delta E(\zeta)_{\text{int}}$ representing the interaction between reactants. So, $\Delta E(\zeta)_{\text{strain}}$ results from the energy required to break the bond and deform bond angles. $\Delta E(\zeta)_{\text{int}}$ results from the bonding capabilities and mutual interaction between the reactants along the reaction coordinate. Considering an S_N1-type reaction mechanism, the analysis will not be between reactants but between carbamic ion and carbocation-CO₂ moieties.

The values of $\Delta E(\zeta)$, $\Delta \Delta E(\zeta)_{\text{strain}}$, and $\Delta \Delta E(\zeta)_{\text{int}}$ were plotted as a function of C2-O2 bond breaking in both *cis* and *trans*-species (Figs. 5D and S14B, respectively). $\Delta \Delta E(\zeta)_{\text{strain}}$ is the sum of the $\Delta E(\zeta)_{\text{strain}}$ for both moieties, while $\Delta \Delta E(\zeta)_{\text{int}}$ corresponds to the change of $\Delta E(\zeta)_{\text{int}}$ as a function of the reaction coordinate. The results for both conformers are in agreement, as $\Delta \Delta E(\zeta)_{\text{strain}}$ is increasingly negative while $\Delta \Delta E(\zeta)_{\text{int}}$ is increasingly positive.

More importantly, this approach demonstrates that the increase of $\Delta E(\zeta)$ along the reaction coordinate is mainly determined by $\Delta \Delta E(\zeta)_{\text{int}}$, as the interaction between the carbamic ion and carbocation-CO₂ moieties become increasingly unfavorable ($\Delta \Delta E(\zeta)_{\text{int}}$ up to 143.0 kcal mol⁻¹). Thus, we can conclude that there is significant interaction between the two moieties of the studied carbamic-carbonic anhydride **4**, which stabilizes the molecule thus hindering its decomposition by C2-O2 bond breaking.

Upon reaching this conclusion, we further decomposed the interaction energy (ΔE_{int}) between the two moieties for the *cis*-species (Table 1), at geometries with C2-O2 bond lengths of 1.36 and 2.46 Å, into a steric (ΔE_{steric}) and orbital interaction energy (ΔE_{orb}) terms.

Table 1. Energy decomposition of the interaction energy (ΔE_{int} , in kcal mol⁻¹) between the carbamic ion and carbocation-CO₂ moieties of the *cis* species of the carbamic-carbonic anhydride **4**, into orbital interaction (ΔE_{orb} , in kcal mol⁻¹) and steric (ΔE_{steric} , in kcal mol⁻¹) terms. The analysis was made for geometries optimized with fixed C2-O2 bond lengths of 1.36 Å (reactant) and 2.46 Å (fragmentation into the carbamic ion, CO₂, and carbocation moieties, as seen in Fig. 5). The analysis was made with the Multiwfn program,³² and was based on ω B97XD/6-31+G(d,p) calculations.

C2-O2 Bond Length / Å	ΔE_{int}	ΔE_{orb}	ΔE_{steric}
1.36	-164.0	-299.0	134.9
2.46	-21.1	-7.2	-13.9
	$\Delta\Delta E_{\text{int}} = 143.0$	$\Delta\Delta E_{\text{orb}} = 291.8$	$\Delta\Delta E_{\text{steric}} = -148.9$

ΔE_{steric} combines electrostatic interaction and exchange repulsion (related with Pauli repulsion effects) terms, while ΔE_{orb} arises from the mixing of occupied and unoccupied orbitals. This energy decomposition was performed with the Multiwfn program,³² and was based on ω B97XD/6-31+G(d,p) calculations.

The energy decomposition analysis (Table 1) shows that the attractive interaction between fragments of the carbonic anhydride (C2-O2 bond lengths of 1.36 Å) is determined mainly by E_{orb} , which provides significant stabilization for this molecule. On the contrary, ΔE_{steric} provides only repulsive contributions to ΔE_{int} . Interestingly, upon C2-O2 bond breaking, ΔE_{steric} contributes favorably for attractive interactions between the fragments ($\Delta\Delta E_{\text{steric}}$ of -148.9 kcal mol⁻¹). However, this is not enough to offset the significant decrease in the favorable contribution of E_{orb} ($\Delta\Delta E_{\text{orb}}$ of 291.8 kcal mol⁻¹).

Orbital interactions (as $n \rightarrow \pi^*$ and $n \rightarrow \sigma^*$) have attracted growing interest in recent years, as they are widely present in biomolecules, materials, drugs, and can affect their geometry and stability.³³⁻³⁵ These interactions are composed of the delocalization of an oxygen's lone pair (n) over the antibonding π^*/σ^* of a nearby carbonyl C-O bond. Natural bond orbital (NBO) analysis was then performed at the ω B97XD/6-31+G(d,p) level for the *cis* species (Fig. 6), to assess the existence of relevant orbital interactions between the carbamic ion and carbocation-CO₂ fragments, with a focus on the C2-O2 bond.

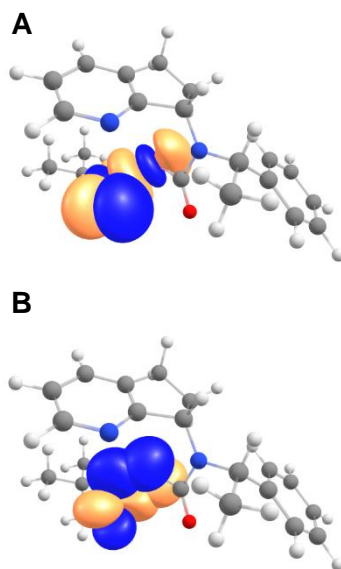


Fig. 6. (A) NBO orbital overlap between oxygen (O3) lone pair of the CO₂ carbonyl moiety of the *cis* species of **4**, and the antibonding σ^* orbital of the C2-O2 bond. (B) NBO orbital overlap between the oxygen (O2) lone pair of the *cis* species of the carbamic-carbonic anhydride, and the antibonding π^* orbital of the C2-O3 carbonyl bond of the CO₂ moiety. Color key: blue = N; red = O; gray = C; white = H.

This analysis showed the occurrence of both $n \rightarrow \pi^*$ and $n \rightarrow \sigma^*$ interactions between the carbamic ion and carbocation-CO₂ moieties. The $n \rightarrow \sigma^*$ interaction consists in significant overlap of the lone pair of O3 and the antibonding σ^* orbital of the adjacent C2-O2 bond (Fig. 6). As for the $n \rightarrow \pi^*$ interaction, it consists of a significant overlap between the lone pair of O2 and the antibonding π^* orbital of the adjacent carbonyl (C2-O3) of the CO₂ moiety. Their associated second-order perturbative energies ($E^{(2)}$) were found to be 44.1 kcal mol⁻¹ for the $n \rightarrow \sigma^*$ interaction and 50.0 kcal mol⁻¹ for the $n \rightarrow \pi^*$ interaction, which indicates a relevant level of stabilization associated with these interactions. More specifically, there appears to be a significant stabilization effect by orbital interactions between fragments, which is associated with the C2-O2 bond. Such orbital interactions are expected to be disrupted if C2-O2 bond-breaking occurs, and so, their stabilizing effect would be lost. This justifies the significant decrease of E_{orb} due to C2-O2 bond breaking (Table 1), which significantly diminishes the attractive interaction between fragments (Fig. 5) and makes the C2-O2 bond-breaking step too energetically demanding, thus preventing its dissociation to form the carbamate **3** and CO₂.

Having provided insight into the surprising stability of **4**, it is also important to rationalize why heating to 140 °C (Fig. 2) yields **2** and not the expected carbamate **3**. It is also relevant to understand why the decomposition of **4** into **2** only occurs with heating to 140 °C, and not also at room temperature. To address the first issue, we calculated the Gibbs free energy differences (with thermal corrections) for the decomposition of the *cis* species of **4** into **2**, isobutene and two CO₂ molecules, at both 25 and 140 °C. These results were compared with values obtained for the decomposition of the *cis* species of **4** into the corresponding carbamate **3** and CO₂ (already referred to above). Both reactions are exothermic at 25 °C in similar magnitudes, with the **4** → **2** reaction being favorable by $-15.0 \text{ kcal mol}^{-1}$, with the **4** → **3** reaction being favorable by $-14.2 \text{ kcal mol}^{-1}$. However, while increasing the temperature did increase the energy difference for both reactions, this increase was significantly higher for the **4** → **2** reaction. Namely, this latter reaction becomes favorable by $-34.3 \text{ kcal mol}^{-1}$, an increase of $-19.2 \text{ kcal mol}^{-1}$. As for the **4** → **3** reaction, it becomes favorable by $-20.9 \text{ kcal mol}^{-1}$, just an increase of $-6.6 \text{ kcal mol}^{-1}$. Thus, we can attribute the formation of **2** as the decomposition product of **4**, upon heating, due to this reaction being significantly more favorable than the thermal decomposition of **4** into the corresponding carbamate **3**.

Nevertheless, these results do put the question of why the decomposition of **4** into **2** does not occur at room temperature. Given the similarity of the results obtained so far for both the **4** → **2** and **4** → **3** reactions, the justification may be related to high energy barriers for different reaction steps. To obtain some corroboration for this, we analyzed the potential energy curve of the N1-C1 bond breaking for the *cis* species of **4**. These types of calculations were performed to obtain a qualitative indication of the stability of a relevant bond that will be broken during the **4** → **2** decomposition. This was done by optimizing the geometries of the conformer at several lengths of the relevant N1-C1 bond. The potential energy curve for the *cis* species is presented in Fig. S15. The results show that N1-C1 bond stretching is associated with a continuous increase in energy up to $81.7 \text{ kcal mol}^{-1}$, with the increase in the N1-C1 bond length from 1.35 to 2.25 Å. Thus, the results do support that dissociation of **4** into the amine **2** is not energetically favorable, further explaining the stability of **4** at 25 °C and why heating up to 140 °C is required for its dissociation with the formation of **2**.

Conclusions

Two chiral carbamic-carbonic anhydrides were synthesized, isolated, and structurally characterized, one of them by single-crystal X-ray diffraction analysis for the first time. The isolation of **4** and **7** provide irrefutable evidence that carbamic-carbonic anhydrides are generated during the reaction between secondary amines and anhydrides in the presence of nucleophilic catalysts. Although DMAP is still widely used as a standard protocol for the preparation of *N*-Boc derivatives, this work draws attention to the formation of carbamic-carbonic anhydrides as stable species (formal side products) rather than “intermediates”. Despite the unfruitful attempts to synthesize *N*-Boc carbamates, the carbamic-carbonic moieties in **4** and **7** are also able to act as an effective *N*-protecting group, being cleaved either by thermolysis (140 °C in the case **4** and 80 °C for **7**) or acidolysis with trifluoroacetic acid to generate the corresponding amines **2** and **6**, respectively. Theoretical calculations conducted for carbamic-carbonic anhydride **4** provided useful insights to rationalize its unusual stability, demonstrating the existence of attractive orbital interactions responsible for holding carbamic ion and carbocation-CO₂ moieties together, making the C2-O2 bond dissociation (necessary for decarboxylation to occur) too energetically demanding. The discovery of the unrecognized role of $n \rightarrow \sigma^*$ orbital interactions in **4** offers useful insights into the stabilization of this functional group, opening a new avenue for the design of new stable carbamic-carbonic anhydrides with potential applications in organic chemistry and related fields.

Experimental Section

General Information. All chemicals described in this work were of reagent grade and used without further purifications. Solvents for chromatography were of reagent grade. CH₂Cl₂ was distilled from CaH₂ under nitrogen and stored over molecular sieves. High-purity grade silica gel used for flash chromatography (Merk 60A, 230-240 mesh) and pre-coated aluminum silica gel plates used for analytical TLC (Merck 60 F₂₅₄, 0.25 mm) were obtained from Merck (Darmstadt, Germany). TLC plates were analyzed under UV radiation and/or by using a solution of phosphomolybdic acid in ethanol requiring gentle heating for visualization. Mass spectra were recorded on an LTQ Orbitrap XL™ hybrid mass spectrometer (Thermo Fischer Scientific, Bremen, Germany) controlled by Xcalibur 2.1.0 and LTQ Tune Plus 2.5.5 (Centro de Materiais da Universidade do Porto, CEMUP). The capillary voltage of the electrospray ionization source (ESI) and the temperature were set to 3.1 kV and 275

°C, respectively, and the sheath gas was set at 6 (arbitrary units) according to the software settings. The capillary and the tube lens voltage were set to 35 V and 110 V, respectively. NMR spectra were recorded at CEMUP with a Bruker Avance III 400 at 400.15 MHz for ^1H and 100.62 MHz for ^{13}C . ^1H and $^{13}\text{C}\{^1\text{H}\}$ chemical shifts are reported (in ppm) and referenced to the residual protic solvent signals (DMSO- d_6 : $\delta_{\text{H}} = 2.50$ and CDCl_3 : $\delta_{\text{H}} = 7.26$) in the ^1H NMR spectra and to the deuterated solvents signals (DMSO- d_6 : $\delta_{\text{C}} = 39.52$ and CDCl_3 : $\delta_{\text{C}} = 77.16$) in the $^{13}\text{C}\{^1\text{H}\}$ NMR spectra. Determination of the optical rotations was performed on a JASCO P-2000 polarimeter (thermostated) and the data was reported as follows: $\alpha_{\text{D}}^{\theta}$ expressed in ($^{\circ}$) (dm^{-1}) (g^{-1}), in which θ is the temperature in Celsius and c ($\text{g} / 100 \text{ mL}$, solvent). Solvents were evaporated using a Büchi rotavapor.

The X-ray intensity data were measured on a Bruker D8 VENTURE PHOTON-III C14 κ -geometry diffractometer system equipped with an Incoatec I μ S 3.0 microfocus sealed tube (Mo $\text{K}\alpha$, $\lambda = 0.71073 \text{ \AA}$) and a multilayer mirror monochromator. The structure was solved and refined using the Bruker SHELXTL Software Package. TGA and DSC were performed on a TGA/DSC 1 STARTe SYSTEM (Mettler-Toledo AG, Schwerzenbach, Switzerland) while using alumina crucibles under a stream of N_2 . The system was operated in the dynamic mode in the temperature range 28-1050 °C. The sample size was 4.3840 mg. The results were processed using the Mettler STARe 9.01 software (Mettler-Toledo AG, Schwerzenbach, Switzerland). FTIR spectrum was recorded on a PerkinElmer Spectrum Two FTIR-ATR instrument from the Department of Chemistry and Biochemistry, Faculty of Sciences of the University of Porto (FCUP|DQB - Lab&Services).

Theoretical Methods. The calculations were performed with the Gaussian 09 program package.³⁶ Geometry optimizations, frequency, and single-point calculations were performed with the wB97XD functional and the 6-31+G(d,p) basis set. wB97XD is a long-range-corrected hybrid exchange-correlation functional that accounts for dispersion effects.³⁷ All calculations were performed in implicit chloroform, which was modeled with the SMD implicit solvation model.³⁸ SMD is based on the integral equation formalism model (IEFPCM), but with radii and nonelectrostatic terms of Truhlar and co-workers' SMD model. Thus, SMD has the advantage of including nonelectrostatic terms in the calculations.³⁸

Synthesis of 2. To a solution of ketone **1** (0.500 g, 3.76 mmol) in CH₂Cl₂ (40 mL) was added (*S*)-1-phenylethan-1-amine (0.73 mL, 5.6 mmol) and anhydrous Na₂SO₄. The suspension was left under magnetic stirring for 4 h at room temperature. After that, NaBH(OAc)₃ (1.193 g, 5.63 mmol) was carefully added and the reaction was further stirred for 20 h. The suspension was filtered under reduced pressure and a saturated solution of NaHCO₃ (aq) (20 mL) was added to the filtrate. The mixture was transferred into a separatory funnel and the aqueous phase was washed with CH₂Cl₂ (3 x 30 mL). The organic extracts were combined and dried over anhydrous Na₂SO₄, filtered, and the solvent removed using a rotavap. The crude oil was chromatographed using EtOAc as eluent, affording amine **2** as a brown oil (0.539 g, 2.26 mmol, 60% yield). TLC (EtOAc): R_f = 0.42; [α]_D²⁰ = -27.9° (c1, CHCl₃). ¹H NMR (CDCl₃, 400 MHz): δ 8.40 (d, *J* = 4.9 Hz, 1H), 7.50–7.41 (m, 3H), 7.36–7.28 (m, 2H), 7.27–7.20 (m, 1H), 7.05 (ddd, *J* = 7.5, 4.9, 0.4 Hz, 1H), 4.25 (q, *J* = 6.6 Hz, 1H), 4.12 (t, *J* = 7.7 Hz, 1H), 2.80 (ddd, *J* = 16.1, 8.8, 2.9 Hz, 1H), 2.73–2.45 (m, 2H), 1.97 (dtd, *J* = 12.8, 7.8, 3.0 Hz, 1H), 1.60 (ddd, *J* = 17.1, 12.8, 8.8 Hz, 1H), 1.48 (d, *J* = 6.6 Hz, 3H). ¹³C{¹H} NMR (CDCl₃, 101 MHz): δ 165.2, 147.8, 146.0, 136.7, 132.7, 128.8, 127.5, 127.2, 122.3, 62.3, 58.6, 33.6, 28.2, 24.5.

Synthesis of 4. To a solution of amine **2** (0.180 g, 0.755 mmol) in CH₂Cl₂ (20 mL) was added catalytic amounts of DMAP followed by Boc₂O (0.181 g, 0.831 mmol), and the reaction was kept stirring for 4 h. The solution was then transferred into a separatory funnel and washed with a saturated solution of NaHCO₃ (aq) (3 x 40 mL). The organic phase was dried over anhydrous Na₂SO₄, filtered, and the solvent removed using a rotavap. The crude oil was then chromatographed with EtOAc affording carbamic-carbonic anhydride **4** as an off-white solid (0.184 g, 0.481 mmol, 64% yield). mp = 109.16 °C; TLC (*n*-hexane:Et₂O, 1:3 v/v): R_f = 0.62; [α]_D²³ = -149° (c1.37, CHCl₃). ¹H NMR (CDCl₃, 400 MHz, conformers 50:50): δ 8.37 (br s, 1H), 7.77 – 7.65 (m, 2H), 7.52 – 7.32 (m, 3H), 7.31 – 7.22 (m, 1H), 7.04 (dd, *J* = 13.1, 4.6 Hz, 1H), [5.59 (d, *J* = 6.0 Hz), 5.30 (d, *J* = 6.0 Hz), 1H], [4.70 (t, *J* = 7.7 Hz), 4.60 (t, *J* = 7.7 Hz), 1H], 3.18 – 2.96 (m, 1H), 2.78 (dd, *J* = 15.3, 7.3 Hz, 1H), 2.57 – 2.20 (m, 2H), [1.76 (d, *J* = 6.3 Hz), 1.72 (d, *J* = 6.3 Hz), 3H], [1.45 (s), 1.30 (s), 9H]. ¹³C{¹H} NMR (CDCl₃, 101 MHz, conformers): δ 162.0, 160.9, 150.0, 148.8, 148.2, 147.6, 147.1, 146.7, 140.0, 136.3, 135.0, 133.2, 132.4, 128.5, 128.4, 128.0, 127.8, 127.6, 127.5, 122.3, 121.9, 84.6, 83.7, 61.1, 60.1, 57.0, 55.6, 31.4, 29.5, 28.2, 27.8, 27.5, 27.5, 19.4, 18.3. HRMS (ESI-TOF) *m/z* calcd for C₂₂H₂₇N₂O₄⁺: 383.19653; found: 383.19656.

Synthesis of 6. Following the same protocol described for the synthesis of **2**, ketone **5** (0.513 g, 3.88 mmol) was reacted with (*S*)-1-phenylethan-1-amine (0.75 mL, 5.8 mmol) followed by the addition of NaBH(OAc)₃ (1.230 g, 5.822 mmol). After typical workup, the crude oil was chromatographed using CH₂Cl₂/MeOH (50:1) as eluent, affording amine **6** as a colourless oil (0.589 g, 2.48 mmol, 64% yield). TLC (CH₂Cl₂/MeOH 50:1): R_f = 0.25; ¹H NMR (CDCl₃, 400 MHz, mixture of diastereoisomers 93:7): δ 7.67 – 7.06 (m, 9 H), [4.32 (dd, *J* = 5.7, 3.6 Hz, minor), 4.18 (t, *J* = 6.6 Hz, major), 4.15 (q, *J* = 6.5 Hz, major), 4.11 – 4.02 (m, minor), 2H], 2.99 (ddd, *J* = 15.9, 8.3, 5.1 Hz, 1H), 2.76 (ddd, *J* = 15.8, 8.1, 7.0 Hz, 1H), [2.46 (dddd, *J* = 11.9, 8.2, 6.8, 3.7 Hz, minor), 2.27 (dddd, *J* = 12.3, 8.2, 7.1, 5.1 Hz, major), 1H], 1.76 (dddd, *J* = 12.8, 8.3, 7.0, 6.1 Hz, 1H), 1.56 (d, *J* = 1.7 Hz, 1H, NH), 1.43 (d, *J* = 6.6 Hz, 3H). ¹³C{¹H} NMR (CDCl₃, 101 MHz): δ 146.6, 146.4, 146.1, 143.6, 143.3, 128.6, 127.4, 127.0, 126.9, 126.4, 126.2, 124.9, 124.6, 124.2, 124.1, 61.2, 60.7, 35.2, 34.2, 30.4, 25.7, 24.8.

Synthesis of 7. Following the same protocol described for the synthesis of **4**, amine **6** (0.173 g, 0.729 mmol) was reacted with catalytic amounts of DMAP followed by the addition of Boc₂O (0.191 g, 0.875 mmol). After typical workup, the crude oil was chromatographed using EtOAc as eluent, affording carbamic-carbonic anhydride **7** as a colourless solid (0.186 g, 0.488 mmol, 67% yield). TLC (EtOAc): R_f = 0.75; [α]_D¹⁷ = –101° (c0.955, CHCl₃). ¹H NMR (CDCl₃, 400 MHz, conformers 71:29): δ 7.61 – 7.28 (m, 5H), 7.24 – 6.89 (m, 3H), [6.62 (d, *J* = 7.3 Hz), 6.43 (d, *J* = 7.3 Hz), 1H], [5.73 (d, *J* = 6.0 Hz), 5.28 (q, *J* = 7.2 Hz), 1H], [4.88 (t, *J* = 7.8 Hz), 4.72 (t, *J* = 8.3 Hz), 1H], 3.15 (ddd, *J* = 16.0, 10.1, 4.0 Hz, 1H), 2.83 (dt, *J* = 16.3, 8.3 Hz, 1H), [2.58 – 2.36 (m), 2.27 (ddt, *J* = 13.7, 10.0, 7.1 Hz), 2H], [1.73 (d, *J* = 7.1 Hz), 1.69 (d, *J* = 7.2 Hz), 3H], [1.51 (s), 1.26 (s), 9H]. ¹³C{¹H} NMR (CDCl₃, 101 MHz, conformers): δ 150.4, 148.0, 146.9, 143.1, 142.6, 141.9, 141.1, 140.5, 140.3, 128.7, 128.7, 128.6, 128.1, 128.0, 127.8, 127.6, 127.5, 126.5, 126.3, 124.7, 124.5, 123.5, 123.4, 84.6, 83.7, 77.4, 60.5, 59.5, 55.7, 54.8, 32.5, 30.95, 31.0, 27.6, 27.4, 18.3, 17.1. HRMS (ESI-TOF) *m/z* calcd for C₄₆H₅₄N₂O₈Na⁺ [2M + Na]⁺: 785.37724; found: 785.37939.

Data availability

Copies of the NMR spectra for compounds (*S,S*)-**2**, **4**, **6**, and **7**. HRMS spectrum for **4** and **7**, and crystallographic data and structure refinement for **4** can be found as part of the ESI (PDF), including FAIR data, with the primary NMR FID files, for all compounds (ZIP).

Accession Codes

CCDC 1410888 contains the supplementary crystallographic data for this paper. These data can be obtained free of charge via www.ccdc.cam.ac.uk/data_request/cif, or by emailing data_request@ccdc.cam.ac.uk, or by contacting The Cambridge Crystallographic Data Centre, 12 Union Road, Cambridge CB2 1EZ, UK; fax: +44 1223 336033.

Author Contributions

I.E.S.-D. conceived and designed the experiments; I.E.S.-D., C.A.D.S., and S.C.S.-R. performed the experiments; L.P.S. performed the computational calculations; I.E.S.-D., C.A.D.S., X.G.-M., L.P.S., and J.E.R.-B. analyzed the data; I.E.S.-D. and L.P.S. wrote the paper. All authors approved the final version of the manuscript.

Conflicts of Interest

There are no conflicts to declare.

Funding

Thanks are due to Fundação para a Ciência e Tecnologia (FCT, Portugal) for funding our Research Unit (ref. UIDB/50006/2020) and the project PTDC/BIA-MIB/29059/2017. I.E.S.-D. and L.P.S. thank FCT for the Stimulus of Scientific Employment, Individual Support (2020.02311.CEECIND/CP1596/CT0004 and CEECIND/01425/2017, respectively). S.C.S.-R. thanks FCT for the Ph.D. scholarship with reference SFRH/BD/147463/2019. FCT is also acknowledged for funding the projects UIDB/00081/2020 (CIQUP), UIDB/05748/2020 (GreenUPorto), and PTDC/QUI-QFI/2870/2020.

Acknowledgments

The authors thank Mariana Andrade (CEMUP), Sílvia Maia (CEMUP), and Cláudia Alves (FCUP|DQB - Lab&Services) for the technical assistance with the NMR, HRMS, and FTIR experiments, respectively.

References

1. D. S. Kemp and T. P. Curran, Base-catalyzed epimerization behavior and unusual reactivity of *N*-substituted derivatives of 2,5-dicarbalkoxypyrrolidine. Preparation of a novel mixed carbamic carbonic anhydride by a 4-(dimethylamino)pyridine-catalyzed acylation, *J. Org. Chem.*, 1988, **53**, 5729-5731.
2. Y. Basel and A. Hassner, Di-*tert*-butyl dicarbonate and 4-(dimethylamino)pyridine revisited. Their reactions with amines and alcohols¹, *J. Org. Chem.*, 2000, **65**, 6368-6380.
3. C. S. Dean and D. S. Tarbell, Reactions of amines, alcohols, and pivalic acid with di-*tert*-butyl dithiol tricarbonates and di-*tert*-butyl tricarbonates, *J. Org. Chem.*, 1971, **36**, 1180-1183.
4. I. J. Bruno, J. C. Cole, P. R. Edgington, M. Kessler, C. F. Macrae, P. McCabe, J. Pearson and R. Taylor, New software for searching the Cambridge Structural Database and visualizing crystal structures, *Acta Crystallogr., Sect. B: Struct. Sci.*, 2002, **58**, 389-397.
5. P. Cidalia Silva, S. Sofia, A. Fabio Rizzo, M. Xerardo Garcia and E. Borges, Synthesis of new propargylated 1-pyrindane derivatives as Rasagiline analogues, *Synlett*, 2013, **24**, 837-838.
6. F. Rizzo-Aguiar, C. A. D. Sousa, X. Garcia-Mera and J. E. Rodríguez-Borges, Synthesis and characterization of 1-pyrindane derivatives as rasagiline analogues, *Chem. Data Collect.*, 2016, **5-6**, 21-27.
7. C. A. D. Sousa, I. E. Sampaio-Dias, F. Rizzo-Aguiar, X. Garcia-Mera and J. E. Rodríguez-Borges, Enantiopure synthesis of 7-(1-pyrindanyl)propargyl ethers as rasagiline analogues via chemical or enzymatic resolution of 1-pyrindan-7-ol, *RSC Adv.*, 2015, **5**, 104509-104515.
8. P. Neves, L. S. Nogueira, A. A. Valente, M. Pillinger, I. S. Gonçalves, I. E. Sampaio-Dias, C. A. D. Sousa, F. Rizzo-Aguiar and J. E. Rodríguez-Borges, Performance of chiral tetracarbonylmolybdenum pyrindanyl amine complexes in catalytic olefin epoxidation, *J. Organomet. Chem.*, 2018, **858**, 29-36.

9. S. V. Chankeshwara and A. K. Chakraborti, Catalyst-free chemoselective *N*-*tert*-butyloxycarbonylation of amines in water, *Org. Lett.*, 2006, **8**, 3259-3262.
10. Yeung, S. Hong and E. J. Corey, A short enantioselective pathway for the synthesis of the anti-influenza neuramidase inhibitor Oseltamivir from 1,3-butadiene and acrylic acid, *J. Am. Chem. Soc.*, 2006, **128**, 6310-6311.
11. R. Downham, F. W. Ng and L. E. Overman, Asymmetric construction of the diazatricyclic core of the marine alkaloids Sarains A–C, *J. Org. Chem.*, 1998, **63**, 8096-8097.
12. T. Mita, N. Fukuda, F. X. Roca, M. Kanai and M. Shibasaki, Second generation catalytic asymmetric synthesis of Tamiflu: Allylic Substitution Route, *Org. Lett.*, 2007, **9**, 259-262.
13. H. Tian, Q. Xia, Q. Wang, J. Dong, Y. Liu and Q. Wang, Direct α -monofluoroalkenylation of heteroatomic alkanes via a combination of photoredox catalysis and hydrogen-atom-transfer catalysis, *Org. Lett.*, 2019, **21**, 4585-4589.
14. J. Dong, Q. Xia, X. Lv, C. Yan, H. Song, Y. Liu and Q. Wang, Photoredox-mediated direct cross-dehydrogenative coupling of heteroarenes and amines, *Org. Lett.*, 2018, **20**, 5661-5665.
15. M. Günther, J. Lategahn, M. Juchum, E. Döring, M. Keul, J. Engel, H. L. Tumbrink, D. Rauh and S. Laufer, Trisubstituted pyridinylimidazoles as potent inhibitors of the clinically resistant L858R/T790M/C797S EGFR mutant: targeting of both hydrophobic regions and the phosphate binding site, *J. Med. Chem.*, 2017, **60**, 5613-5637.
16. E. Brambilla, V. Pirovano, M. Giannangeli, G. Abbiati, A. Caselli and E. Rossi, Gold-catalyzed cascade reactions of 4*H*-furo[3,2-*b*]indoles with propargyl esters: synthesis of 2-alkenylidene-3-oxoindolines, *Org. Chem. Front.*, 2019, **6**, 3078-3084.
17. K. L. Granberg, Z.-Q. Yuan, B. Lindmark, K. Edman, J. Kajanus, A. Hogner, M. Malmgren, G. O'Mahony, A. Nordqvist, J. Lindberg, S. Tångefjord, M. Kossenjans, C. Löfberg, J. Brånalt, D. Liu, N. Selmi, G. Nikitidis, P. Nordberg, A. Hayen, A. Aagaard, E. Hansson, M. Hermansson, I. Ivarsson, R. Jansson-Löfmark, U. Karlsson, U. Johansson, L. William-Olsson, J. Hartleib-Geschwindner and K. Bamberg, Identification of mineralocorticoid receptor modulators with low impact on electrolyte homeostasis but maintained organ protection, *J. Med. Chem.*, 2019, **62**, 1385-1406.

18. A. Elmabruk, B. Das, D. Yedlapudi, L. Xu, T. Antonio, M. E. A. Reith and A. K. Dutta, Design, Synthesis, and pharmacological characterization of carbazole based dopamine agonists as potential symptomatic and neuroprotective therapeutic agents for Parkinson's disease, *ACS Chem. Neurosci.*, 2019, **10**, 396-411.
19. M. G. Bursavich, C. W. West and D. H. Rich, From peptides to non-peptide peptidomimetics: design and synthesis of new piperidine inhibitors of aspartic peptidases, *Org. Lett.*, 2001, **3**, 2317-2320.
20. P. Cheng and D. L. J. Clive, Formation of optically pure cyclic amines by intramolecular conjugate displacement, *J. Org. Chem.*, 2012, **77**, 3348-3364.
21. Y. Gao, D. Shan and Y. Jia, Intramolecular Larock indole synthesis for the preparation of tricyclic indoles and its application in the synthesis of tetrahydropyrroloquinoline and fargesine, *Tetrahedron*, 2014, **70**, 5136-5141.
22. The crystallographic data of 4 have been deposited at the Cambridge Crystallographic Data Centre as supplementary publication number CCDC 1410888.
23. E. Guibé-Jampel and M. Wakselman, An easy preparation of the water-soluble *t*-butoxycarbonylating agent 1-Boc-4-dimethylaminopyridinium tetrafluoroborate, *Synthesis*, 1977, **1977**, 772-772.
24. H.-J. Knölker, T. Braxmeier and G. Schlechtingen, A novel method for the synthesis of isocyanates under mild conditions, *Angew. Chem., Int. Ed. Engl.*, 1995, **34**, 2497-2500.
25. P. Molina, M. Alajarin, P. Sanchez-Andrada, J. Elguero and M. L. Jimeno, A new and efficient preparation of cyclic carbodiimides from bis(iminophosphoranes) and the system Boc₂O/DMAP, *J. Org. Chem.*, 1994, **59**, 7306-7315.
26. D. S. Tarbell, Carboxylic carbonic anhydrides and related compounds, *Acc. Chem. Res.*, 1969, **2**, 296-300.
27. D. S. Tarbell and N. A. Leister, The stability of mixed carboxylic-carbonic anhydrides, *J. Org. Chem.*, 1958, **23**, 1149-1152.
28. L. P. Wolters and F. M. Bickelhaupt, The activation strain model and molecular orbital theory, *Wiley Interdiscip. Rev. Comput. Mol. Sci.*, 2015, **5**, 324-343.
29. D. H. Ess and K. N. Houk, Distortion/interaction energy control of 1,3-dipolar cycloaddition reactivity, *J. Am. Chem. Soc.*, 2007, **129**, 10646-10647.

30. F. Liu, Y. Liang and K. N. Houk, Bioorthogonal cycloadditions: computational analysis with the distortion/interaction model and predictions of reactivities, *Acc. Chem. Res.*, 2017, **50**, 2297-2308.
31. F. M. Bickelhaupt and K. N. Houk, Analyzing reaction rates with the distortion/interaction-activation strain model, *Angew. Chem., Int. Ed. Engl.*, 2017, **56**, 10070-10086.
32. T. Lu and F. Chen, Multiwfn: a multifunctional wavefunction analyzer, *J. Comput. Chem.*, 2012, **33**, 580-592.
33. A. Rahim, P. Saha, K. K. Jha, N. Sukumar and B. K. Sarma, Reciprocal carbonyl–carbonyl interactions in small molecules and proteins, *Nat. Commun.*, 2017, **8**, 78.
34. S. K. Singh, K. K. Mishra, N. Sharma and A. Das, Direct spectroscopic evidence for an $n \rightarrow \pi^*$ interaction, *Angew. Chem., Int. Ed.*, 2016, **55**, 7801-7805.
35. J. Sandoval-Lira, J. M. Solano-Altamirano, O. Cortezano-Arellano, S. Cruz-Gregorio, R. L. Meza-León, J. M. Hernández-Pérez and F. Sartillo-Piscil, Can an $n(\text{O}) \rightarrow \pi^*$ interaction provide thermodynamic stability to naturally occurring cephalosporolides?, *J. Org. Chem.*, 2019, **84**, 2126-2132.
36. Gaussian 09, Revision D.01, M. J. Frisch, G. W. Trucks, H. B. Schlegel, G. E. Scuseria, M. A. Robb, J. R. Cheeseman, G. Scalmani, V. Barone, G. A. Petersson, H. Nakatsuji, X. Li, M. Caricato, A. Marenich, J. Bloino, B. G. Janesko, R. Gomperts, B. Mennucci, H. P. Hratchian, J. V. Ortiz, A. F. Izmaylov, J. L. Sonnenberg, D. Williams-Young, F. Ding, F. Lipparini, F. Egidi, J. Goings, B. Peng, A. Petrone, T. Henderson, D. Ranasinghe, V. G. Zakrzewski, J. Gao, N. Rega, G. Zheng, W. Liang, M. Hada, M. Ehara, K. Toyota, R. Fukuda, J. Hasegawa, M. Ishida, T. Nakajima, Y. Honda, O. Kitao, H. Nakai, T. Vreven, K. Throssell, J. A. Montgomery, Jr., J. E. Peralta, F. Ogliaro, M. Bearpark, J. J. Heyd, E. Brothers, K. N. Kudin, V. N. Staroverov, T. Keith, R. Kobayashi, J. Normand, K. Raghavachari, A. Rendell, J. C. Burant, S. S. Iyengar, J. Tomasi, M. Cossi, J. M. Millam, M. Klene, C. Adamo, R. Cammi, J. W. Ochterski, R. L. Martin, K. Morokuma, O. Farkas, J. B. Foresman, and D. J. Fox, Gaussian, Inc., Wallingford CT, 2013.
37. J.-D. Chai and M. Head-Gordon, Long-range corrected hybrid density functionals with damped atom–atom dispersion corrections, *Phys. Chem. Chem. Phys.*, 2008, **10**, 6615-6620.

38. A. V. Marenich, C. J. Cramer and D. G. Truhlar, Universal solvation model based on solute electron density and on a continuum model of the solvent defined by the bulk dielectric constant and atomic surface tensions, *J. Phys. Chem. B*, 2009, **113**, 6378-6396.